Proceedings of the 8th International
IEEE Conference on Intelligent Transportation Systems
Vienna, Austria, September 13-16, 2005

Contrast Restoration of Foggy Images through use of an Onboard Camera

Nicolas Hautière
LIVIC - INRETS / LCPC
building 824, 14 route de la Minière
78000 Versailles, France
nicolas.hautiere@lcpc.fr

Didier Aubert
LIVIC - INRETS / LCPC
building 824, 14 route de la Minière
78000 Versailles, France
didier.aubert@inrets.fr

Abstract— **Perception sensors (cameras, laser, radar) are being introduced into certain vehicles. These sensors have been designed to operate within a wide range of situations and conditions (weather, luminosity, etc.) with a prescribed set of variation thresholds. Effectively detecting when a given operating threshold has been surpassed constitutes a key parameter in the creation of driving assistance systems that meet required reliability levels. With this context in mind, an atmospheric visibility measurement system may be capable of quantifying the most common operating range of onboard exteroceptive sensors. In particular, foggy images suffer from poor contrast. Furthermore, this decay varies across the scene and is exponential in the depths of scene points. In this paper, we present a physics based method to restore contrast of foggy images without any a priori weather-specific prediction. Our method only uses a simple black-and-white camera mounted onboard a moving vehicle. Furthermore, we are able to estimate the meteorological visibility distance, which characterizes the weather condition.**

I. Vision and poor visibility conditions

Under bad weather conditions, the contrast of images is drastically degraded. An atmospheric visibility measurement system may be taking weather effects into account to create a vision system more reliable. A first solution is to adapt the system or to deactivate it momentarily if an operating threshold have been surpassed. A second solution is to remove weather effects from the image. Unfortunately, this decay varies across the scene and is exponential in the depths of scene points. Consequently, space invariant filtering techniques fail to adequately remove weather effects from images.

The majority of sensors dedicated to measuring visibility distances (diffusiometer, transmissometer) are expensive to operate and quite often complicated to install correctly. Moreover, this type of equipment cannot easily be placed onboard a vehicle. Use of a camera however does not entail any such obstacles, even though admittedly this topic has only received minimal attention in the literature. Bush [1] and Kwon [2] relied upon a fixed camera placed above the roadway for the purpose of measuring visibility distances. Systems that entail use of an onboard camera however are encountered much less frequently. Only Pomerleau [3] estimates visibility by means of measuring the contrast attenuation of road markings at various distances in front of a moving vehicle.

On the opposite, methods which restore image contrast under bad weather conditions are much more encountered in the literature. Unfortunately, they have all of them rather strong constraints in order to be onboard a moving vehicle. Some techniques require prior information about the scene [4]. Others require dedicated hardware in order to estimate the weather conditions.

Some techniques rely only on the acquired images and exploit the atmospheric scattering to obtain the range map of the scene [5], [6], [7]. However, they require weather conditions to change between image acquisitions. Otherwise, polarization filters techniques can be used to reduce haziness in the image. Unfortunately, they require two differently filtered images of the same scene. This is the case for Schechner [8] who analysed two polarization filtered images taken in bad weather to compute scene structure and dehaze images.

Some techniques assume a flat world scene like [9]. However, the user must manually specify a location for sky region, vanishing point and an approximation of distances distribution in the image. In [10], the authors compute the extinction coefficient of fog and assume a flat world seen from a forward-looking airborne camera. However, they approximate the distribution of radiances in the image with a simple gaussian with known variance.

In this paper, we first present a daylight fog modeling. Then, we present our technique estimating the extinction coefficient of fog in the current image. Once the weather condition is known, we use it to restore the contrast of scene points which respect to the flat world assumption. Our method has less constraints than the previous ones. Indeed, it only needs the presence of the road and the sky in the image to work, restores scene contrast without any a priori weather-specific prediction and runs onboard a moving vehicle.

II. Fog effects on road vision

A. Propagation of light through fog

In the presence of fog, visible light (with a wavelength situated between 400 and 700 nanometers) must be propagated within an aerosol that contains a large number of water droplets. During its trajectory, the light is attenuated by the dual phenomena of absorption and diffusion, which leads to characterizing fog by means of an extinction coefficient β (equal to the sum of the absorption and diffusion

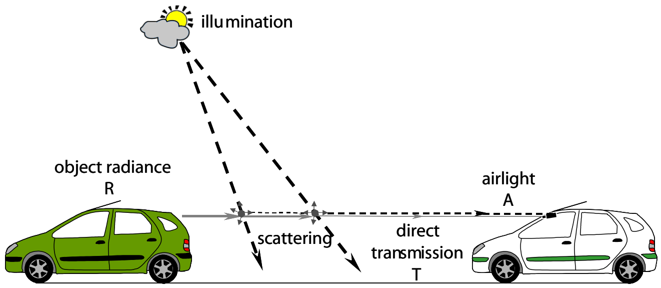

Fig. 1. Fog illumination or haze luminance are due to the daylight scattering. Light coming from the sun and scattered by atmospheric particles towards the camera is the airlight A. The latter increases with the distance. The light emanating from the object R is attenuated by scattering along the line of sight, leading to the direct transmission T. The latter decreases with distance.

coefficients). In reality however, the absorption phenomenon is negligible in this type of aerosol. The predominant phenomenon therefore proves to be diffusion, which acts to deviate light rays from their initial direction. Such is the origin of fog illumination, or haze luminance, a phenomenon so highly characteristic of daytime fog. This effect is illustrated on Fig. 1 and has been described by Dumont in [11].

B. Koschmieder's model

In 1924, Koschmieder [12] proposed his theory on the apparent luminance of objects observed against background sky on the horizon. In noting that a distant object winds up blending in with the sky, he established a simple relationship between the distance d of an object with intrinsic luminance L_o and its apparent luminance L as follows:

$$L = L_0 e^{-\beta d} + L_\infty (1 - e^{-\beta d}) \tag{1}$$

where L_∞ denotes the luminance of the sky and β the extinction coefficient of the atmosphere.

Consequently, the intensity we measure in the image is the sum of the airlight and the direct transmission. So, with the notations of Fig. 1, on the camera the intensity is:

$$I = T + A \tag{2}$$

$$I = Re^{-\beta d} + A_\infty (1 - e^{-\beta d}) \tag{3}$$

where A_∞ is the airlight of an object at the horizon.

Based on these results, Duntley [12] derived an attenuation law of atmospheric contrasts:

$$C = C_0 e^{-\beta d} \tag{4}$$

where C designates the apparent contrast at distance d and C_o the intrinsic contrast of the object against its background.

This law is only applicable in the case of daylight uniform illumination of the atmosphere. In order for the object to be just barely visible, the value of C must equal the contrast threshold ε. From a practical standpoint, the International Commission on Illumination (CIE) [13] has adopted an average value of $\varepsilon = 0.05$ for the contrast threshold so as to define a conventional distance, called the "meteorological visibility distance" V_{met}, i.e. the greatest distance at which a black object ($C_o = 1$) of a suitable dimension can be seen in the sky on the horizon.

$$V_{met} = -\frac{1}{\beta}\ln(0.05) \simeq \frac{3}{\beta} \tag{5}$$

III. Sensor modeling within the vehicle environment

A. Presentation of the sensor used

The sensor used in our set-up is a simple black-and-white camera mounted in back of the vehicle windshield. Fig. 2 sets forth the modeling approach for the sensor within the vehicle environment. In the image reference plane, the position of a pixel is given by its (u,v) coordinates. The coordinates of the optical center projection in the image are designated by (u_0,v_0). θ denotes the angle between the optical axis of the camera and the horizontal, while v_h represents the vertical position of the horizon line. The intrinsic parameters of the camera are its focal length f, and the horizontal size t_{pu} and vertical size t_{pv} of a pixel. We have also made use herein of $\alpha_u = \frac{f}{t_{pu}}$ and $\alpha_v = \frac{f}{t_{pv}}$, and have typically considered: $\alpha_u \approx \alpha_v = \alpha$.

B. Computation model for the depth at a point seen in the image

Given that just a single camera is being used in this approach, we are unable to gain access to image depth. This problem has been overcome by adopting the hypothesis of a flat road, which makes it possible to associate a distance with each line of the image. In the following discussion, we will present this distance computation model.

By applying the pinhole model for the camera, a point with three-dimensional coordinates (x,y,z) within the camera reference system is projected onto the image plane in accordance with the following expression:

$$\begin{cases} u = u_0 + \alpha\frac{x}{z} \\ v = v_0 + \alpha\frac{y}{z} \end{cases} \tag{6}$$

According to Fig. 2, the horizontal line passing through the optical center makes an angle θ with the z-axis of the camera. Within the image plane, the horizon line can therefore be written as:

$$v_h = v_0 - \alpha \tan(\theta) \tag{7}$$

By virtue of Eq. (6), we are able to deduce the following:

$$\frac{v - v_h}{\alpha} = \frac{y}{z} + \tan(\theta) \tag{8}$$

Being positioned within the (S, X, Y, Z) reference corresponding to the scene, Eq. (8) then becomes:

$$\frac{v - v_h}{\alpha} = \frac{Y + H}{Z} - \tan(\theta) \tag{9}$$

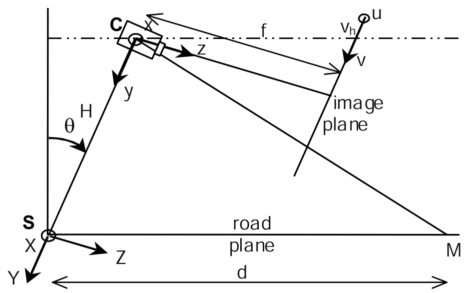

Fig. 2. Modeling of the camera within its environment; it is located at a height of H in the (S,X,Y,Z) coordinate system relative to the scene. Its intrinsic parameters are its focal length f and pixel size t. θ is the angle between the optical axis of the camera and the horizontal. Within the image coordinate system, (u,v) designates the position of a pixel, (u_0,v_0) the position of the optical center C, and v_h the vertical position of the horizon line.

A point M located on the road at distance d from the origin S gets parameterized as:

$$M \begin{pmatrix} X \\ -d\sin(\theta) \\ d\cos(\theta) \end{pmatrix} \tag{10}$$

It can then be deduced that:

$$\frac{v - v_h}{\alpha} = \frac{H}{d\cos(\theta)} \tag{11}$$

The distance d can ultimately be expressed by:

$$d = \begin{cases} \frac{\lambda}{(v - v_h)} & \text{if } v > v_h \\ \infty & \text{if } v \leq v_h \end{cases} \tag{12}$$

where $\lambda = \frac{H\alpha}{\cos(\theta)}$.

C. Calibration of the sensor

Using the model presented in Fig. 2, a simple estimation of the value of parameter λ makes it possible to calibrate the sensor. To perform this step, knowing the actual distance $d_1 - d_2$ between two points and their coordinates v_1 and v_2 in the image proves sufficient (cf. Fig. 3). By virtue of Eq. (12), we are ultimately able to obtain the following:

$$\lambda = \frac{d_1 - d_2}{\left(\frac{1}{v_1 - v_h} - \frac{1}{v_2 - v_h}\right)} \tag{13}$$

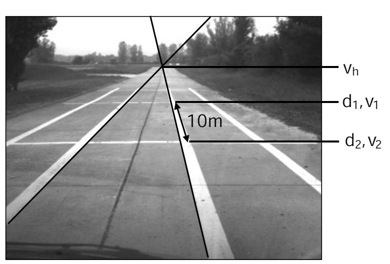

Fig. 3. Example of image used for sensor calibration captured on our calibration site. v_1 and v_2 are the lines representing two objects located at distances d_1 and d_2, respectively. v_h is the line representing the focus point in the image.

As part of an initial approach, the horizon line position v_h can be obtained by searching the focus point in the image of road markings, sidewalks, etc. Such an installation has been proposed in [14].

IV. Estimation of the weather condition

A. Theoretical framework

In section II, we presented Koschmieder's model. This section is devoted to studying the mathematical properties of this formula as well as deducing the existence of an inflection point capable of being detected on the image and providing a basis for our solution.

Following a variable change from d to v based on Eq. (12), Eq. (3) then becomes:

$$I = R - (R - A_\infty)(1 - e^{-\beta \frac{\lambda}{v - v_h}}) \tag{14}$$

By taking the derivative of Eq. (14) with respect to v, the following is obtained:

$$\frac{dI}{dv} = \frac{\beta\lambda(R - A_\infty)}{(v - v_h)^2} e^{-\beta \frac{\lambda}{v - v_h}} \tag{15}$$

By once again taking the derivative of I with respect to v, we obtain the following:

$$\frac{d^2 I}{dv^2} = \beta\varphi(v) e^{-\beta \frac{\lambda}{v - v_h}} \left(\frac{\beta\lambda}{v - v_h} - 2 \right) \tag{16}$$

where $\varphi(v) = \frac{\lambda(R - A_\infty)}{(v - v_h)^3}$.

The equation $\frac{d^2 I}{dv^2} = 0$ has two solutions. The solution $\beta = 0$ is of no interest to the present discussion. The only useful solution therefore is given in Eq. (17):

$$\beta = \frac{2(v_i - v_h)}{\lambda} = \frac{2}{d_i} \tag{17}$$

where v_i denotes the position of the inflection point and d_i its distance to the camera. In this manner, the parameter β of Koschmieder's model is obtained once v_i is known.

Moreover, Eq. (17) displays the remarkable property $\lim_{v_i \to v_h} \beta = 0$, which can serve to detect the presence of fog. If v_i is greater than v_h, fog will indeed be detected; otherwise, it can be deemed that no fog is present.

By virtue of both Eqs. (5) and (17), we are able to deduce the meteorological visibility distance V_{met}:

$$V_{met} = \frac{3\lambda}{2(v_i - v_h)} \tag{18}$$

Furthermore, based on the v_i, v_h and β values, we are able to deduce the other parameter values of Eq. (3) through use of I_i and $\frac{dI}{dv}_{|v=v_i}$, which are respectively the values of the function I and its derivative in $v = v_i$:

$$R = I_i - (1 - e^{-\beta d_i}) \frac{(v_i - v_h)}{2e^{-\beta d_i}} \frac{dI}{dv}_{|v=v_i} \tag{19}$$

$$A_\infty = I_i + \frac{(v_i - v_h)}{2} \frac{dI}{dv}_{|v=v_i} \tag{20}$$

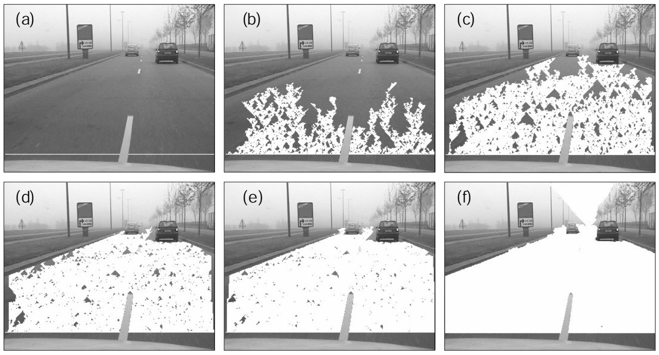

Fig. 4. Various results of the region growing as a function of parameter set values $\{G_{max}^{-1}\ G_{max}^{0}\ G_{max}^{1}\}$ (a) expansion seeds, (b) {1,1,1} (c) {1,2,1} (d) {2,3,2} (e) {3,5,3} (f) {5,8,5}

B. Method implementation

To implement Koschmieder's model, we measure the median intensity on each line of a vertical band. So as to be in accordance with Koschmieder's model assumptions, this band should only take into account a homogeneous area and the sky.

Thus, we identify a region within the image that displays minimal line-to-line gradient variation G_{max} when crossed from bottom to top, in a configuration that allows for compatibility with Koschmieder's model. From this perspective, the seeds of region expansion are chosen as the pixels of a line from the bottom of the image whose gray level lies close to the median of gray levels for this line.

Given the position and optical characteristics of the camera, the majority of pixels in this line represent in fact the road surfacing layer. As such, just the road pixels have been taken into account, as indicated in Fig. 4, thus avoiding for example the increase in certain seeds on a road marking. Similarly, only the three pixels lying above the current pixel $\tilde{P}$ (see Fig. 5) can be incorporated into the target region. This technique makes it possible to circumvent those objects not to be included within the target region.

Fig. 4 presents various results from region expansion procedures for different values of G_{max}. To the extent possible, region expansion continues until the top of the image has been reached. Even though we did not explicitly intend to focus on road as well as sky, it turns out that the region detected by this algorithm contains a portion of both these elements, as Fig. 6 also depicts.

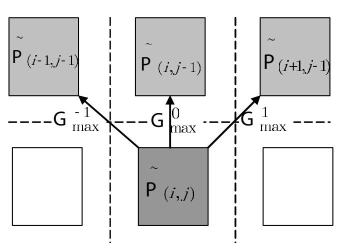

Fig. 5. Diagram representative of the condition of aggregation of a pixel to the target region in its 8-vicinity.

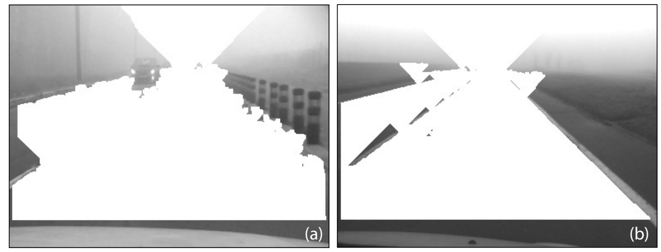

Fig. 6. Results of the region growing on our test images.

Once the segmentation is achieved, there are two possibilities. If the region growing did not cross the image from bottom to top, the system is said to be inoperative and the computation is stopped on this image.

In the contrary case, the implementation of Koschmieder's model is possible. A vertical band must be located in the detected area, so as to avoid taking measurement on low contrasted objects which may be falsely integrated within the area, generally the road edges. In this purpose, we search the most vertical way to go from bottom to top of the image.

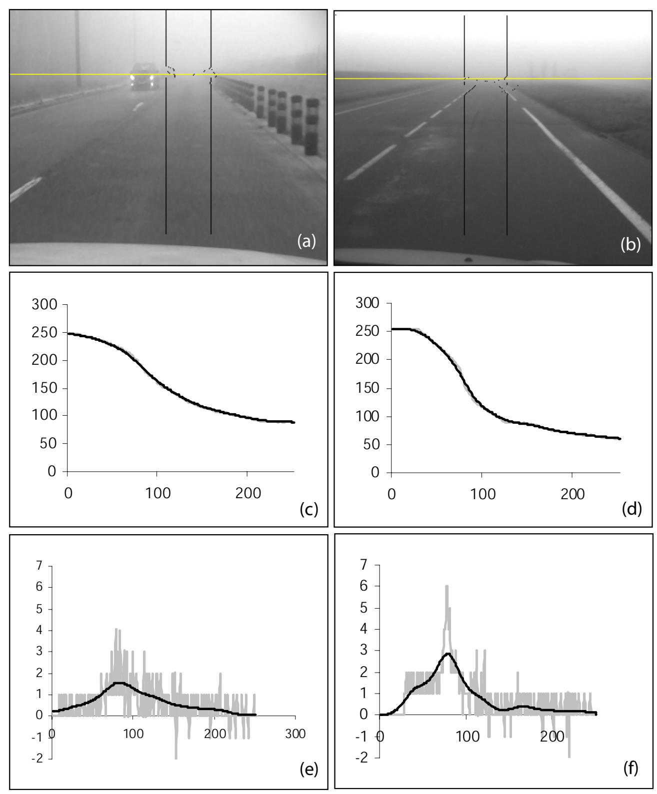

Fig. 7. (a)(b): Examples of measurement bandwidth computations (black lines) and of visibility distances (horizontal lines) under foggy conditions. (b)(c): curves representative of the measurement of vertical intensity variation in the image. (c)(d) depict the derivatives of these curves (gray - without smoothing; black - with smoothing).

This way constitutes the center of the vertical band of measure which is deployed on both sides of it until the desired width is obtained or until the region border is reached.

Finally, we can measure the median intensity on each line of the vertical band, which allows us to obtain the vertical variation of the intensity of the image (cf. Fig. 7) and deduce the parameters of Eq. (3) (cf. IV-A).

V. CONTRAST RESTORATION

In this section, we describe a simple method to restore scene contrast from an image of a foggy scene. Consider a point P belonging to the image. Its intensity I is given by Koschmieder's model:

$$I = Re^{-\beta d} + A_\infty(1 - e^{-\beta d}) \tag{21}$$

where R is the point radiance without atmospheric perturbation. (A_∞, β) characterize the weather condition and are known thanks to section IV. Consequently, we can recover R directly:

$$R = Ie^{\beta d} + A_\infty(1 - e^{\beta d}) \tag{22}$$

with $\beta d = 2\frac{v_i - v_h}{v - v_h}$ and $A_\infty = I_i + \frac{v_i - v_h}{2}\frac{dI}{dv}_{|v=v_i}$.

The procedure is repeated independently for each pixel of the image. Since R is independent of the weather condition, we have restored the contrast of the scene using just one image without previous knowledge of the scene and of the weather condition. However, the contrast is correctly restored only on points which respect the flat world assumption (see Section III). This is not the case for vertical objects near the sensor.

VI. METHOD EVALUATION

We performed experiments with real scenes (respectively 200 and 1000 images). Fig. 9a was grabbed using a Sony DCR-TRV50E Digital Video Camera Recorder. Fig. 9b was grabbed using a Sony XC-8500CE camera. Both video sequences have been taken under dense fog conditions. To assess the performance of our method, we propose to evaluate first the measurement of the extinction coefficient of fog. Then, we propose to measure the scene contrast before and after the contrast restoration.

A. Measurement of the extinction coefficient β of fog

Fig. 6 shows the results of the region growing process described in Section IV-B. Fig. 7 shows the results of bandwidth computation and measurement of vertical intensity variation in the image as well as its derivative. The line representative of visibility distance is also presented. On Fig. 8, the measurement of visibility proves to be stable despite the presence of obstacles, which tends to show the good properties of our method. Recently, we have equipped a test site with six large reference targets, located between 30m and 200m from the cameras onboard the stationed vehicle. The tests conducted reveal a good accuracy of the technique and are published in [15].

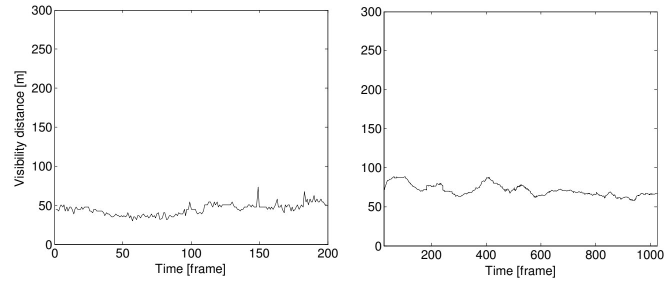

Fig. 8. Meteorological visibility distance measurements conducted on both image sequences (200 and 1000 images); vertical axis: visibility distance in meters - horizontal axis: frame number.

B. Computation of contrasts above 5 %

Köhler's technique [16] used to binarize an image finds the threshold which maximized the contrast between two parts of the image. Let f be a gray level image. A couple of pixels (x,x_1) is said to be separated by s if two conditions are met. First, $x_1 \in V_4(x)$. Secondly, the condition (23) is respected:

$$\min(f(x), f(x_1)) \leq s < \max(f(x), f(x_1)) \tag{23}$$

Let $F(s)$ be the set of all couples (x, x_1) separated by s, such as $x \in V_4(x_1)$. With these definitions, for every value of s belonging to [0,255], $F(s)$ is built. For every couple belonging to $F(s)$, the logarithmic contrast [17] $C_{x,x_1}(s)$ is computed:

$$C_{x,x_1}(s) = \min\left(\frac{|s - f(x)|}{\max(s, f(x))}, \frac{|s - f(x_1)|}{\max(s, f(x_1))}\right) \tag{24}$$

The mean contrast (25) associated to $F(s)$ is then performed:

$$C(s) = \frac{1}{\text{card}(F(s))}\sum_{(x,x_1)\in F(s)} C_{x,x_1}(s) \tag{25}$$

The best threshold s_0 verifies the following condition:

$$C(s_0) = \max_{s\in[0,255]} C(s) \tag{26}$$

It is the threshold which has the best mean contrast along the associated border $F(s_0)$. Instead of using this method to binarize images, we use it to measure the contrast locally. The evaluated contrast is then equal to $2C(s_0)$ along the associated border $F(s_0)$.

$$C_{x,x_1}(s) = \min\left(\frac{|s - f(x)|}{\max(s, f(x))}, \frac{|s - f(x_1)|}{\max(s, f(x_1))}\right) \tag{27}$$

C. Results

Results of experiments are shown on Figs. 9 and 10. The fog was removed using the algorithm mentioned in Section V. On Fig. 9b, notice that the contrast on the second crossed vehicle is restored. On Fig. 10b, trees have become visible and road markings are visible further. Subjective results are confirmed by Figs. 9d and 10d. Contrasts above 5 % are detected further on restored images than on the original images. Consequently, visibility distance has been increased. The method has been tested on our experimental prototype. The whole process is performed within 40 ms with a current-day PC.

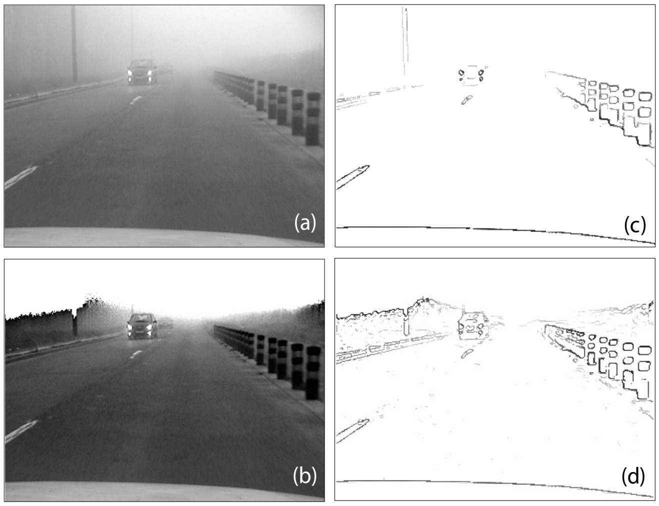

Fig. 9. (a) Image captured using a Sony DCR-TRV50E Digital Video Camera Recorder under dense fog conditions. The instrumented vehicle crosses two other vehicles. Only the first vehicle is really visible. No contrast above 5 % is detected on the second vehicle, as we can see on (c). On the contrary, on (b) the first vehicle became more contrasted. Now the second vehicle is detected, as we can see on (d). Road markings are also better perceived on (d).

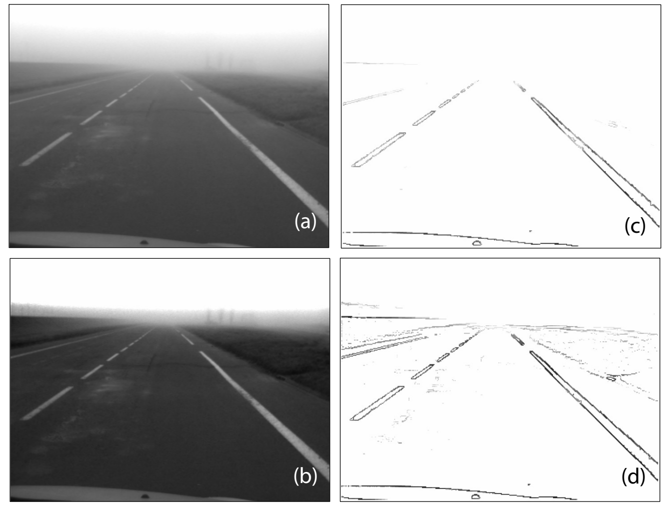

Fig. 10. (a) Image captured using a Sony XC-8500CE camera under dense fog conditions. Very few points with contrast above 5 % are detected on (c). On (b), we are able to perceive the road in a better way. Some trees that were not visible on (a) are visible on (b). This is also the case for the road markings. The subjective feeling is confirmed by (d).

VII. Conclusion

In this paper, we presented a method to restore the contrast of foggy images through use of an onboard camera. Such a system is useful for detecting road markings or objects on the road further in adverse conditions, wether it is made by human vision or by image processing. Thanks to an instantiation of Koschmieder's model, we are able to detect fog and to estimate the meteorological visibility distance. Our method needs only the presence of the road and the sky in the image to run. Once the weather condition is known, we use it to restore the contrast of scene points which respect to the flat world assumption. The whole process is performed within 40ms using a Pentium IV 2.4 GHz. We evaluated the method thanks to different video sequences. In order to evaluate the performances of our methods and to calibrate them, we have built targets so as to provide a reference measure of the atmospheric diffusion. We are also investigating a technique working on non flat world.

Acknowledgments

The authors would like to acknowledge the contribution of Éric Dumont, Jean-Philippe Tarel (LCPC) and Michel Jourlin, (Univ. of Saint-Étienne). This work is partly founded by the French ARCOS project [18]. The process of visibility distance estimation has been patented [19].

References

[1] C. Bush and E. Debes, "Wavelet transform for analyzing fog visibility," *IEEE Intelligent Systems*, vol. 13, no. 6, pp. 66–71, November/December 1998.

[2] T. M. Kwon, "Atmospheric visibility measurements using video cameras: Relative visibility," University of Minnesota Duluth, Tech. Rep., July 2004.

[3] D. Pomerleau, "Visibility estimation from a moving vehicle using the ralph vision system," in *IEEE Conference on Intelligent Transportation Systems*, November 1997, pp. 906–911.

[4] J. P. Oakley and B. L. Satherley, "Improving image quality in poor visibility conditions using a physical model for contrast degradation," in *IEEE Transactions on Image Processing*, no. 7, 1998, pp. 167–179.

[5] S. G. Narasimhan and S. K. Nayar, "Removing weather effects from monochrome images," in *IEEE Conference on Computer Vision and Pattern Recognition*, December 2001.

[6] ——, "Contrast restoration of weather degraded images," *IEEE Transactions on Pattern Analysis and Machine Intelligence*, vol. 25, no. 6, pp. 713–724, June 2003.

[7] F. Cozman and E. Krotkov, "Depth from scattering," in *IEEE Conference on Computer Vision and Pattern Recognition*, June 1997.

[8] Y. Y. Schechner, S. G. Narasimhan, and S. K. Nayar, "Instant dehazing of images using polarization," in *IEEE Conference on Computer Vision and Pattern Recognition*, December 2001.

[9] S. G. Narashiman and S. K. Nayar, "Interactive deweathering of an image using physical model," in *IEEE Workshop on Color and Photometric Methods in Computer Vision*, 2003.

[10] J. P. Oakley, B. L. Satherley, C. G. Harrison, and C. S. Xydeas, "Enhancement of image sequences from a forward-looking airborne camera," in *Proc. SPIE Vol. 2666, p. 266-276, Image and Video Processing IV, Robert L. Stevenson; M. Ibrahim Sezan; Eds.*, mars 1996, pp. 266–276.

[11] E. Dumont, "Characterization, modelling and simulation of fog effects on road vision," Ph.D. dissertation, Paris V university, November 2002.

[12] W. Middelton, *Vision through the atmosphere*. University of Toronto Press, 1952.

[13] *International lighting vocabulary*. Commission Internationale de l'Éclairage, 1987, no. 17.4.

[14] J.-P. Tarel, D. Aubert, and F. Guichard, "Tracking occluded lane-markings for lateral vehicle guidance," in *IEEE CSCC'99*, 1999.

[15] N. Hautière, D. Aubert, and E. Dumont, "Onboard measurement of the atmospheric visibility: Static calibration and quantitative evaluation," in *17th TRB Biennial Symposium on Visibility and Traffic Control Devices, Washington, USA*, April 2005.

[16] R. Köhler, "A segmentation system based on thresholding," *Graphical Models and Image Processing*, vol. 15, pp. 319–338, 1981.

[17] M. Jourlin and J.-C. Pinoli, "Logarithmic image processing," *Advances In Imaging and Electron Physics*, vol. 115, pp. 129–196, 2001.

[18] PREDIT, "ARCOS: Research Action for Secure Driving. [http://www.arcos2004.com]."

[19] J. Lavenant, J.-P. Tarel, and D. Aubert, "Procédé de détermination de la distance de visibilité et procédé de détermination de la présence d'un brouillard," Brevet français 0201822 soumis par LCPC / INRETS, Février 2002.